Copper-promoted cobalt/titania nanorod catalyst for CO hydrogenation to hydrocarbons

Wasim U. Khan[a], Xuemin Li[a], Luqmanulhakim Baharudin[b] and Alex C.K. Yip[a,*]

[a]Department of Chemical and Process Engineering, College of Engineering, University of Canterbury, Christchurch, New Zealand.

[b]Faculty of Chemical Engineering, Universiti Teknologi MARA, 40450 Shah Alam, Selangor, Malaysia.

* Corresponding author: Alex C.K. Yip (alex.yip@canterbury.ac.nz)

Abstract

The effect of Cu on cobalt/titania nanorod (Co/TNR) catalysts for the promotion of carbon monoxide (CO) hydrogenation to hydrocarbons was investigated. Varying amounts of Cu (1.5-6.0 wt%) were loaded onto the base Co/TNR catalyst using the deposition-precipitation method. Characterization by X-ray diffraction (XRD) revealed that the Cu particles were well dispersed over the Co/TNR catalysts. Characterizations by temperature-programmed desorption of hydrogen (H_2-TPD) and carbon monoxide (CO-TPD) and temperature-programmed reduction in hydrogen (H_2-TPR) proved the effect of the Cu promoter in the Co/TNR catalyst by its bimetal effect with Co, where the Co/TNR catalysts containing Cu generally showed a significant improvement in comparison with the base Co/TNR catalyst not containing the Cu promoter. The CO and H_2 adsorption capacities and reducibility were optimal on the catalyst containing 1.5% Cu (1.5Cu-Co/TNR). This aligns well with the catalytic activity performance of all the catalysts, where the 1.5Cu-Co/TNR catalyst exhibited

the best performance, yielding 16.8% CO conversion and 57.7% C_{5+} hydrocarbon selectivity at 240 ℃ and 5 bar.

Keywords: Cocatalysts; Cu promoter; Co; Titania nanorods; CO hydrogenation.

1 Introduction

Fischer-Tropsch synthesis (FTS) is a well-known process of hydrocarbon production from synthesis gas or syngas (H_2 + CO) [1-4]. Biomass, coal and natural gas are among the carbon-containing feedstock or potential sources of syngas. The hydrogen-to-carbon monoxide (H_2/CO) ratio in the syngas and the extent of impurities vary with the source of feedstock. In addition, for the biomass or coal feedstock, the H_2/CO ratio also depends on the gasification technology used in the syngas production process [2].

It is imperative to note that the quality of the FTS products is not dependent on the source of the syngas feedstock, but is a function of catalyst selection and operating conditions. The metals that have been reported to show catalytic activity in FTS are Fe, Ru, Ni and Co [5]. Among these metals, only Fe and Co are commercially used for FTS due to the good trade-offs between catalyst cost, activity, stability and selectivity they offer [6-12]. An important aspect of using Fe- and Co-based catalysts in FTS is their catalytic activity towards the water-gas shift (WGS) reaction that generates CO_2 and H_2 from the reaction between water and CO in the feedstock, which affects the H_2/CO ratio during the FTS process. Co-based catalysts are less active towards the low-temperature WGS reaction, making them preferable for the FTS of hydrogen-rich syngas, typically derived from natural gas [13, 14]. Fe-based catalysts, on the other hand, are suitable for the FTS of hydrogen-lean (or CO-rich) syngas, typically derived from biomass or coal [15, 16]. Of Fe and Co, the former is less expensive and offers strong

resistance to poisons such as hydrogen sulfide and sulfur-containing thiophene [8], but the latter is preferable for the production of large hydrocarbons such as diesel (C_{12}–C_{20}) [6]. High stability and high selectivity of the catalysts towards heavy hydrocarbons are especially desirable for FTS [17], making Co-based catalysts better candidates for this process.

In FTS using Co-based catalysts, the Co metal is prone to deactivation by mechanisms such as metal agglomeration or sintering, coke or carbon formation during the reaction, poisoning and reoxidation of the Co metal particles [18, 19]. Sulfur has a significant contribution as a poisoning agent because it binds strongly to the metal active sites and causes electronic modifications to neighbor atoms. leading to deactivation of the catalyst [20]. In addition, minimization of the surface energy of the Co crystallites promotes metal agglomeration, which results in catalyst deactivation due to the reduced active surface area. Moreover, under conditions where water is produced as a byproduct, the Co active sites are reoxidized to Co oxides that are inactive for FTS [20]. Therefore, the effects of promoters on enhancing the activity, selectivity and stability of Co-based catalysts in FTS have been explored [21]. For example, the sintering of Co particles, which is one of the main causes of catalyst deactivation, can be controlled by the use of a textural promoter [1]. Ma *et al*. [22] investigated copper promotion over activated carbon (AC)-supported 15.7 wt% Fe and 0.9 wt% K catalysts. It was revealed that while copper addition of up to 2 wt% enhanced the reducibility of iron oxide, this improvement did not have any significant impact on the catalytic activity in the FTS process.

Jacobs *et al*. [23] studied the effect of three promoters (Cu, Au and Ag) over a 15 wt% Co/Al_2O_3 catalyst. The addition of small fractions (up to 2.7 wt%) of these promoters improved the reducibility of the Co catalysts. In the case of Ag- and Au-promoted Co catalysts, the density of the active sites was observed to have been enhanced. However, excess amounts of promoters proved to be detrimental and resulted in decreased activity due to reduced accessibility of the reactant gases to the Co active sites that were covered by the excess promoters.

In heterogeneous catalysis, titania (TiO_2) is used in different nanostructured forms, including nanotubes (TNT), nanorods (TNR), nanobelts and nanowires. TNT and TNR have been considered useful supports in heterogeneous catalysis due to their unique characteristics of large specific surface area, large pore volume, ion exchangeability and rapid electron transport competency [24-26]. In our recent work [27], the role of TNR-supported copper-based catalysts was investigated for CO oxidation, in which the Cu–TNR metal–support interactions and interfacial active sites were proven to have a profound impact on the catalytic performance.

Although copper is widely used as an effective promotor in WGS reactions, the synergistic effect of the Cu-Co interaction over titania nanorods (TNR) and its specific performance on the hydrocarbon selectivity have not been reported in detail. In the current work, TNR-supported Co catalysts containing varying amounts of Cu were prepared and tested in CO hydrogenation reactions to investigate the role of Cu as the catalyst promoter. Characterization techniques such as CO-TPD, H_2-TPD and H_2-TPR were used to elucidate the bimetal effect of Cu and Co.

2 Experimental

2.1 Catalyst preparation

Copper-promoted, titania nanorod (TNR)-supported cobalt catalysts were synthesized using the deposition-precipitation method. The chemicals used were copper acetate (Sigma Aldrich®), cobalt acetate (Sigma Aldrich®), TNR and 1 M sodium carbonate (Na_2CO_3) solution. First, the TNR were synthesized (the procedure has been reported elsewhere [27]). Then, the cobalt solution was prepared. For 1 g of catalyst, 0.225 g of cobalt acetate was dissolved in deionized water and stirred until a clear solution was attained, followed by the

addition of 0.925 g of TNR to the cobalt precursor solution. A 1 M Na_2CO_3 solution was added to the catalyst solution dropwise until a pH value of 10 was reached. Then, the solution was kept under magnetic stirring for 12 h followed by filtration and washing of the samples three times using deionized water. The samples were oven-dried at 120 ℃ for 12 h followed by calcination in air at 400 ℃ for 5 h. The base catalyst, denoted as Co/TNR, contained 7.5 wt% of Co. A similar procedure was adopted to synthesize Cu-promoted catalysts. For 1 g of Cu-promoted Co/TNR catalysts, copper precursor solutions of various concentrations were prepared by dissolving 0.0475, 0.0950 and 0.1900 g of copper acetate in deionized water. A specific amount of base Co/TNR catalyst was added to the solution to give Cu-promoted Co/TNR catalysts with Cu loadings of 1.5, 3.0 and 6.0 wt%. The Cu-promoted catalysts are denoted as xCu-Co/TNR, where x = Cu loading content in wt%.

2.2 Catalyst characterization

X-ray diffraction (XRD) patterns were recorded using a Philips PW1700 X-ray diffractometer (Co-Kα radiation source). The recordings were obtained for a scanning range of 20-80° with a scanning step of 0.05°. MPI Jade® software was used for XRD data analysis.

Temperature-programmed reduction with hydrogen (H_2-TPR) and temperature-programmed desorption using CO and H_2 (CO-TPD and H_2-TPD, respectively) were conducted in a BELCAT II chemisorption apparatus. For the H_2-TPR measurements, the catalyst surface was pretreated by keeping 35-40 mg of the catalyst sample at 200 ℃ for half an hour under an inert atmosphere (helium flow of 30 mL/min). The sample was subsequently cooled to ambient temperature before it was heated to 500 ℃ at 10°C/min under analysis gas (5% H_2/Ar mixture) flowing at 30 mL/min. The reduced samples were further used for CO- and H_2-TPD. Prior to CO- and H_2-TPD experiments, the sample that had gone through the H_2-TPR was degassed

with helium flow of 50 ml/min. The sample was then heated from ambient temperature to 100 °C for 20 min, in which the temperature was maintained at 100 °C for 15 min. The temperature was decreased to 50 °C for CO (or H_2) adsorption. The adsorption of CO and H_2 was carried out at 50 °C using a 10%CO/He mixture (30 mL/min) and a 5%H_2/Ar mixture (30 mL/min), respectively. The profiles of the desorption of the CO and H_2 probe gases were recorded by a thermal conductivity detector (TCD) while raising the sample temperature at a rate of 10 °C/min to 500 °C in helium flowing at 30 mL/min.

2.3 CO hydrogenation over Cu-promoted Co/TNR catalysts

The CO hydrogenation reaction was carried out in a fixed bed tubular reactor. The catalyst was placed over glass beads, and the temperature of the catalyst bed was monitored using a K-type thermocouple. A total of 100 mg of each catalyst was loaded into the reactor and activated at 350 °C for 5 h with a pure (100%) hydrogen flow (10 ml/min) at 1.5 bar prior to reaction. After catalyst reduction, hydrogen was replaced with Ar, and the temperature was decreased to the reaction temperature (240-300 °C). The reactor was then pressurized to 5 bar using Ar, and then the reaction feed gas (10 mL/min) with a H_2/CO ratio of 2, balanced with Ar, was fed into the reactor. The products and unconverted reactants were analyzed using a gas chromatograph (SRI Instruments) equipped with a flame ionization detector (FID) and a TCD. Data were collected at a time-on-stream of 60 min. The CO conversion and product selectivity were calculated using the following equations:

$$CO\ Conversion\ [X_{CO}]\ (\%) = \frac{CO_{in} - CO_{out}}{CO_{in}} \times 100 \quad (1.1)$$

$$S_{Cx\%} = \frac{n_x \times n_C}{CO_{in} - CO_{out}} \quad (1.2)$$

where X_{CO} is the conversion of CO, n_x is the number of moles of product x, and n_C is the number of carbon atoms in product x. The mass balance was applied based on the number of moles of carbon converted into the products.

3 Results and Discussion

3.1 Characterizations

The crystalline structure and nature of the catalyst phase were identified using powder XRD. The XRD patterns in Fig. 1 show that the Cu-promoted Co/TNR catalysts have similar crystalline structures with a mixture of characteristic rutile and anatase phases. It is worth noting that no characteristic peak of either Cu or Co or its oxides is observed for any of the catalysts, which suggests well-dispersed metal particles over the TNR surface [28-30].

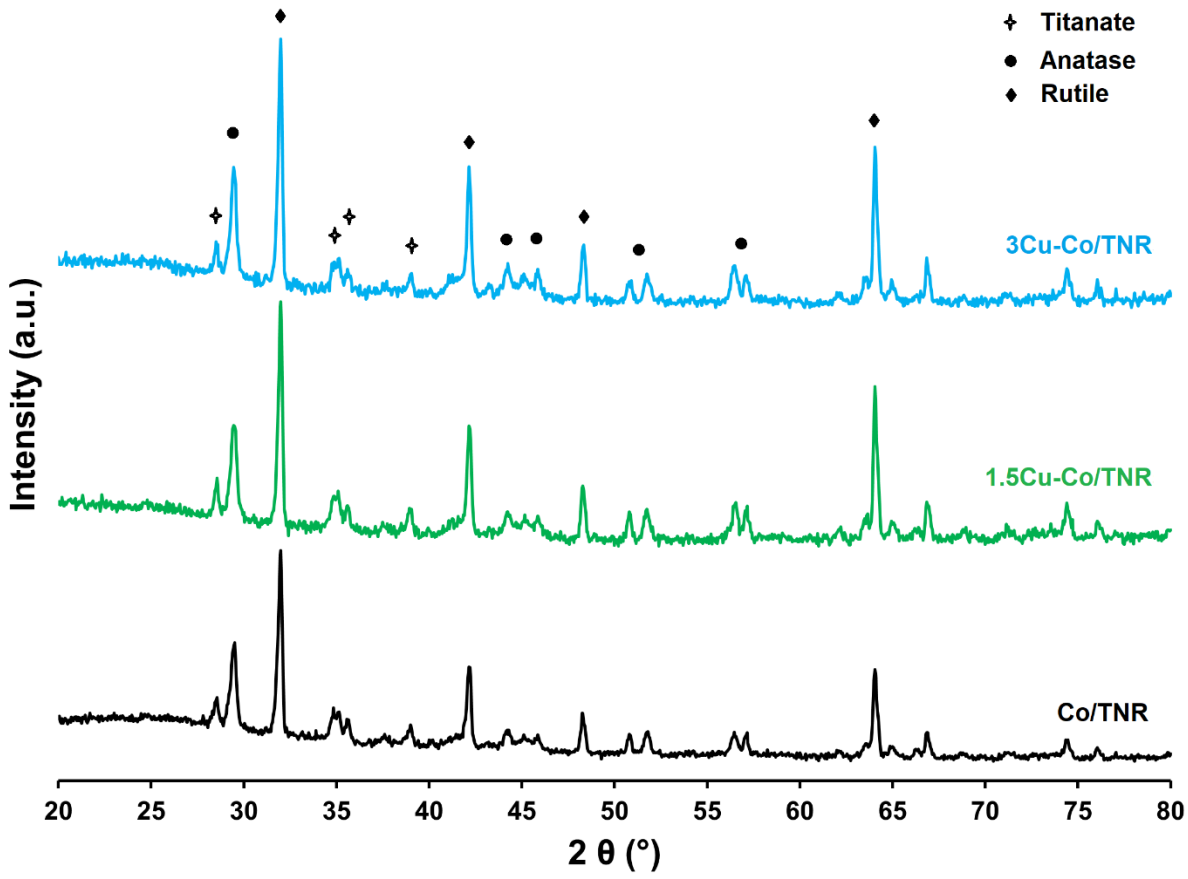

Fig. 1 XRD patterns of the Cu-promoted Co/TNR catalysts.

CO-TPD and H_2-TPD were carried out to study the interaction between the probe gases and the catalyst surface. Fig. 2 shows CO desorption profiles for the Co/TNR catalysts with the different amounts of Cu. The desorption profiles can be divided into two regions; region I ranges from 60 to 260 ℃, and region II ranges from 260 to 450 ℃. In region I, a broad desorption peak is observed for all the catalysts, in which the peak temperature varies with the Cu amount. The desorption peak temperature increases from 110 ℃ for the base Co/TNR catalyst to 180 ℃ when a small fraction of Cu (1.5Cu-Co/TNR) is present. The desorption peak temperature further increases to 200 ℃ when 3 wt% Cu (3Cu-Co/TNR) is anchored over the Co/TNR. Interestingly, the desorption peak temperature decreases to 125 ℃ for the 6Cu-Co/TNR catalyst. It is generally accepted that CO adsorption over Cu is weaker than that over

Co [31], but interestingly, the results show that the smaller fraction of Cu in the Cu-promoted catalyst (1.5Cu-Co/TNR) results in a significant increase in the peak intensity, and the desorption peak shifts towards a higher temperature than that of the base Co/TNR catalyst. This suggests an interaction effect between the Cu and Co metals.

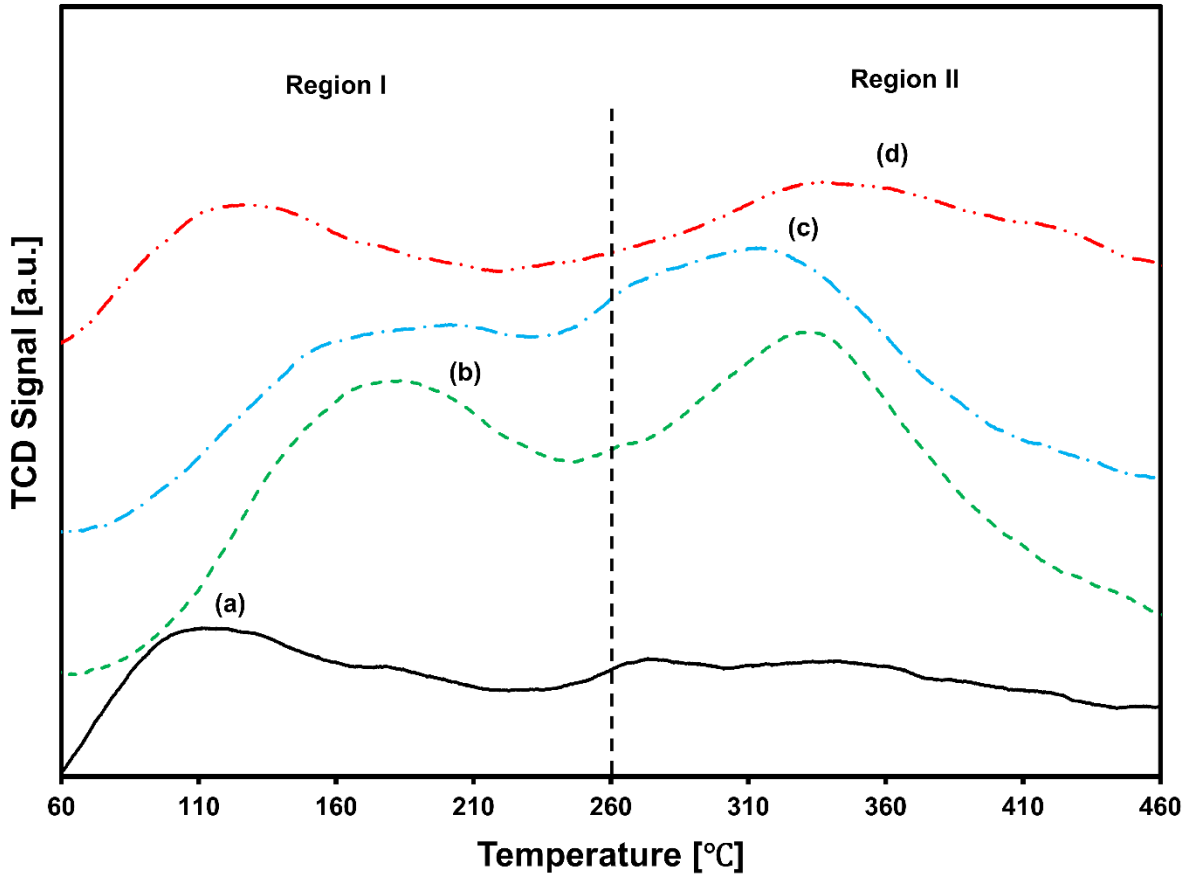

Fig. 2 CO-TPD profiles of the Cu-promoted Co/TNR catalysts: a) Co/TNR, b) 1.5Cu-Co/TNR, c) 3Cu-Co/TNR, and d) 6Cu-Co/TNR.

The desorption profiles in region II exhibit a slightly different trend than those in region I. A very broad peak is observed over the base Co/TNR catalyst with a temperature maximum at ~280 ℃, which shifts to a higher temperature (335 ℃) after the addition of 1.5% Cu (1.5Cu-Co/TNR). It is worth noting that a further increase in Cu (3Cu-Co/TNR) resulted in a decrease in the desorption peak temperature to 315 ℃, but the desorption peak temperature increased to

340 ℃ upon a further increase in the Cu content to 6.0% (6Cu-Co/TNR). This shift in the desorption peak temperature, which indicates the strength of interaction between CO and the catalyst surface (i.e., a lower desorption peak temperature indicates a lower desorption activation energy, which indicates a weaker interaction, and vice versa) [32], is different from that of the CO adsorption capacity of the catalysts. The quantitative results presented in Table 1 show that in general, the addition of Cu increases the CO amount adsorbed on the Co/TNR catalyst. However, although the adsorbed CO amount spikes when 1.5% Cu is present in the Co/TNR catalyst, the adsorption amount decreases with a further increase in the Cu content.

Table 1 Quantitative results of CO and H_2 adsorption.

Catalyst	CO adsorbed (μmol/g)[a]	H_2 adsorbed (μmol/g) [b]
Co/TNR	130	40
1.5Cu-Co/TNR	480	130
3Cu-Co/TNR	469	80
6Cu-Co/TNR	350	50

[a] From CO-TPD; [b] From H_2-TPD

To gain insight into the catalyst surface's response to hydrogen adsorption, the H_2-TPD profiles shown in Fig. 3 were analyzed. The base Co/TNR catalyst exhibits hydrogen desorption with maxima at 120, 180, 260, 345 and 425 ℃, indicating the presence of various active sites for adsorption of H_2 molecules over the whole temperature spectrum. The addition of 1.5% Cu drastically modified the adsorption active sites, where a high and broad peak at a peak temperature of 170 ℃ was observed. Additionally, two narrow-shouldered but notable peaks are observed at approximately 360 and 410 ℃. The 3Cu-Co/TNR catalyst shows H_2 desorption

peaks at 135, 170, 280, 345 and 400 ℃, while the 6Cu-Co/TNR catalyst displays H_2 desorption profiles with peak maxima at 115, 220, 265, 350 and 450 ℃.

The adsorbed H_2 amount calculated from the area under the curves of the H_2-TPD profiles (Fig. 3) is given in Table 1. Similar to the CO adsorption capacity, Cu promotion results in a higher H_2 adsorption capacity than that observed for the Co/TNR catalyst, which could be ascribed to the bimetal effect of Cu and Co. The 1.5Cu-Co/TNR catalyst exhibits the highest H_2 adsorption amount of 130 μmol/g, which is over three times the amount adsorbed on the base catalyst. A further increase in the Cu content (3Cu-Co/TNR and 6Cu-Co/TNR) resulted in a further reduction in the amount of H_2 adsorption (80 and 50 μmol/g, respectively) on the catalysts, implying that an overloading of Cu resulted in a decreased H_2 adsorption capacity. The position at which H_2 is adsorbed on the Cu-Co/TNR catalysts could be determined in detail via theoretical studies, such as density functional theory (DFT) calculations, the density of states (DoS) and molecular dynamics (MD) simulations.

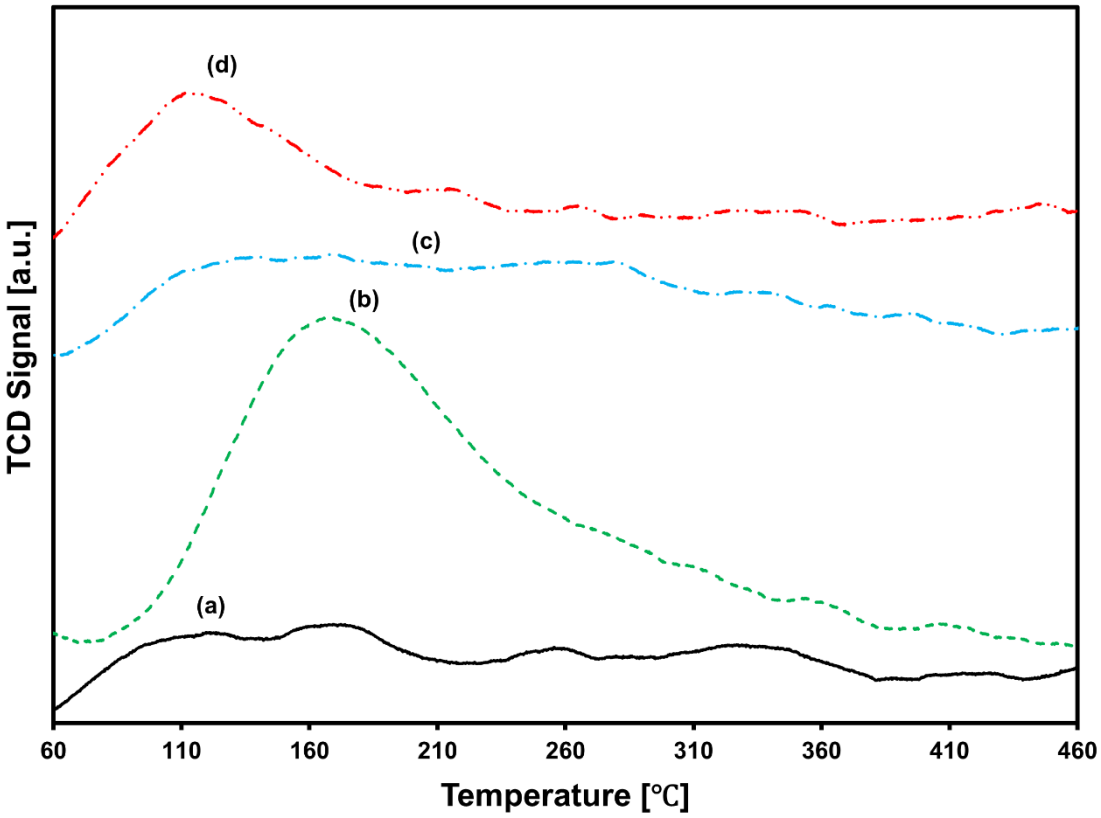

Fig. 3 H_2-TPD profiles of the Cu-promoted Co/TNR catalysts: a) Co/TNR, b) 1.5Cu-Co/TNR, c) 3Cu-Co/TNR, and d) 6Cu-Co/TNR.

H_2-TPR was performed to determine the extent of surface reducibility and the interaction between the metal and the support of the catalysts, which are important parameters for evaluating their catalytic performance in heterogeneous catalysis. The reduction profiles for the base and the Cu-promoted Co/TNR catalysts are shown in Fig. 4. The reduction of Co_3O_4 has been reported to be a complex process, in which the reduction is generally affected by the particle size, Co dispersion and homogeneity of the catalyst. For instance, large particles weakly interacting with the support or surface oxides are easier to reduce [33]. The reduction profiles of the base Co/TNR catalyst presented in Fig. 4 exhibit two reduction peaks with peak temperatures of 300 (peak I) and 405 ℃ (peak II). The reduction of the Co oxides can be explained from a couple of different perspectives. First, peak I at the lower temperature can be

assigned to the reduction of the Co_3O_4 having a weak interaction with the TNR support, while peak II at the higher temperature can be assigned to the reduction of Co_3O_4 and CoO to Co^0 [34]. The other perspective from the literature is based on the ratio of the two peaks. A ratio of peak I to peak II of ~1/3 suggests that the two peaks indicate a two-step reduction of Co_3O_4 to metallic Co by Co_3O_4 ($Co^{2+}.Co_2^{3+}$) → CoO (Co^{2+}) → Co (Co^0) [33, 35].

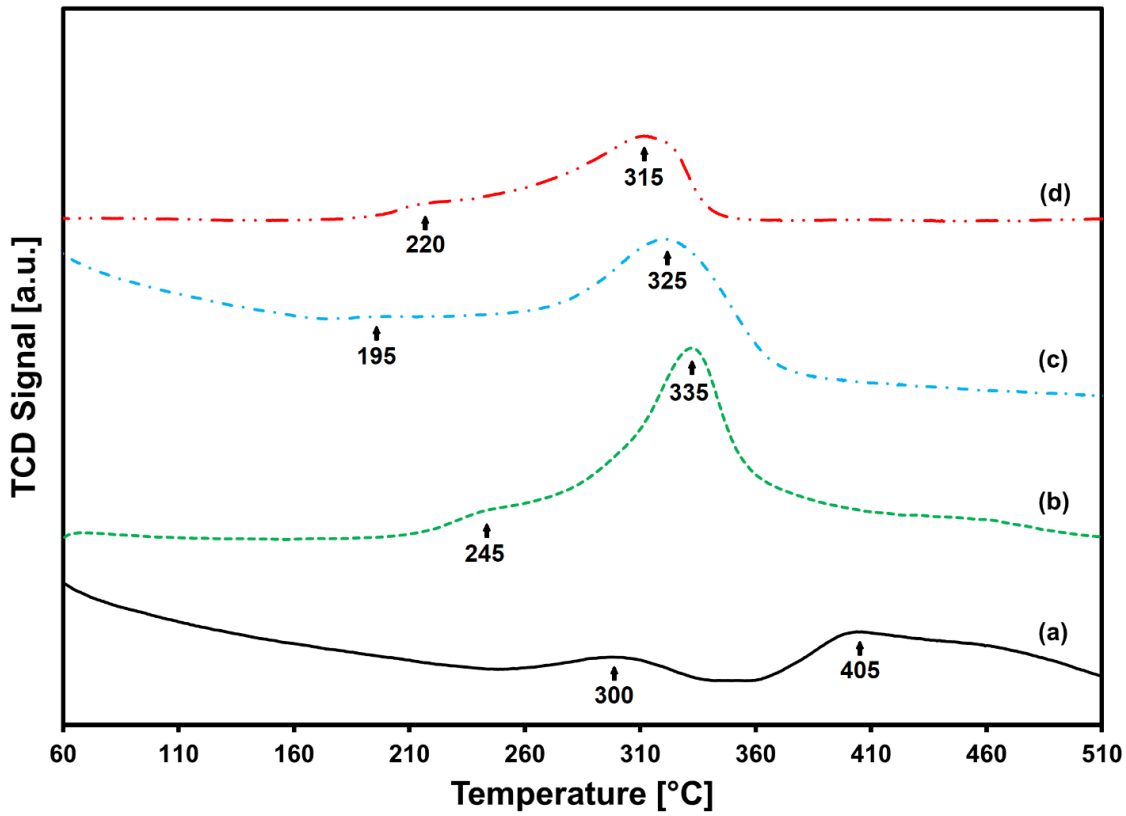

Fig. 4 H_2-TPR patterns for the Cu-promoted Co/TNR catalysts: a) Co/TNR, b) 1.5Cu-Co/TNR, c) 3Cu-Co/TNR, and d) 6Cu-Co/TNR.

It is evident from the H_2-TPR profiles that Cu promotion significantly affects the reducibility of the Co/TNR catalyst. The addition of Cu lowers the reduction peak temperatures from 300 (peak I) and 405 °C (peak II) for the base Co/TNR catalyst to 245 and 335 °C, respectively, for

the 1.5Cu-Co/TNR catalyst. A further increase in the Cu content to 3 wt% (3Cu-Co/TNR) lowers the reduction peak I and peak II temperatures further to 195 and 325 ℃, respectively.

However, the reduction temperature of peak I shifts to the right (220 ℃), while the peak II reduction temperature shifts slightly to the left (315 ℃) for the 6Cu-Co/TNR catalyst. In general, the presence of the Cu improves the reducibility of the base Co/TNR catalyst, where the reduction of Co oxides is enabled at a much lower temperature. Note also that the peak intensities of the promoted catalysts decrease when the Cu contents are (relatively) excessive, which may covers the Co oxide, and hence, results in loss of the Co reducible species. In addition, given that the reduction of TiO_2 is not favourable at temperatures below 500 °C and that the Cu content (approximately 1.5 – 6.0 wt%) is low compared with Co, the effect of TiO_2 or Cu reduction on the H_2-TPR signal is negligible in the tested temperature range (60 °C – 510 °C).

3.2 FTS activity tests

The catalytic performance of the base and the Cu-promoted Co/TNR catalysts for the FTS reaction was investigated at 5 bar and 240 ℃. The results of the catalyst activity (CO conversion) and the product selectivity are presented in Table 2 and Fig. 5. The bare TNR support was first tested under the reaction conditions and did not exhibit any activity for the FTS reaction. The CO conversion of the base Co/TNR catalyst at 240 ℃ was 9.4%. Cu doping significantly influenced the catalytic performance of the catalysts, where the CO conversion increased to 16.8% when 1.5% Cu (1.5Cu-Co/TNR) was present. The activity of the Cu-promoted catalyst, however, deteriorated with the presence of higher contents of the Cu promoter, where the 3Cu-Co/TNR catalyst gave a significant decrease in the CO conversion. A further increase in the Cu content (6Cu-Co/TNR) resulted in a further decrease in the catalyst

activity performance. Based on the CO conversion results, the catalysts are arranged by their activity performance in the following order:

1.5Cu-Co/TNR > 3Cu-Co/TNR > Co/TNR > 6Cu-1Co/TNR

Table 2 The FTS activity and selectivity data for base and Cu promoted Co/TNR catalysts.

Catalyst	Temperature (°C)	CO conv. (%)	Carbon selectivity (%)				
			CH_4	C_2 olefin	C_2-C_4 Paraffins[a]	C_{5+}[a]	CO_2
Co/TNR	240	9.4	26.7	2.5	17.3	51.3	2.2
1.5Cu-Co/TNR		16.8	15.7	2.2	23.4	57.5	1.2
3Cu-Co/TNR		13.3	26.8	2.1	21.7	43.5	5.9
6Cu-Co/TNR		5.7	41.6	-	14.8	18.1	24.9
1.5Cu-Co/TNR	300	25	32.7	0.6	21.5	35.7	9.5
3Cu-Co/TNR		19.6	46.1	0.4	13.5	16.5	23.5

Reduction: 350 °C in pure hydrogen for 4 h, 6000 mL/($g_{cat.}$h); FTS conditions: H_2/CO = 2, 6000 mL/(g_{cat}.h), T= 240 °C, P = 5 bar; [a] gas chromatography mass spectrometry (GCMS) was used to identify the hydrocarbons up to $C_{10.}$ Data were collected at a time-on-stream of 60 min.

It was also found that Cu promotion affects product selectivity. The selectivity of paraffins and C_{5+} hydrocarbons increased from 17.3% and 51.3% over the base Co/TNR catalyst to their highest values (23.4% and 57.5%) over the 1.5Cu-Co/TNR catalyst, but then decreased as the

Cu loading increased, where paraffins and C_{5+} hydrocarbons selectivity of 14.8% and 18.1%, respectively, were obtained with Cu loading of 6%.

In contrast, the selectivity of methane and CO_2 decreased from 26.7% and 2.2% to 15.7% and 1.2%, respectively, when a small amount of Cu was loaded (1.5Cu-Co/TNR). With further increasing of the Cu loading, the selectivity of methane and CO_2 increased and reached 41.6% and 24.9%, respectively, over the 6Cu-Co/TNR catalyst.

It is also interesting to note that the selectivity of C_2 olefin decreased with increasing Cu loading. These results can be explained by the interaction of the reacting gases, *i.e.*, CO and H_2, with the catalyst surface and their contribution towards the FTS reaction before and after the addition of the Cu promoter.

CO dissociative adsorption could be a key step in FTS chain initiation under certain conditions or in the presence of specific metals [36]. In this work, the affinity of CO to the catalyst surface likely plays a significant role during the reaction. The adsorption of CO over the Co surface at room temperature is considered nondissociative in either linear or bridged form [37]. Linear-type CO desorption occurs at 77 ℃, while bridged-type CO desorbs at 167 ℃ *via* a disproportionation reaction ($2CO \rightarrow C + CO_2$) [38, 39]. This suggests that the desorption peak in the desorption profiles in region I seen in Fig. 2 represents the desorption of a mixture of the linear-type CO, as well as CO_2 that was derived from the bridged-type CO disproportionation. In this work, the chemisorption unit used to perform the TPD experiments was not equipped with a mass spectrometer. Due to this limitation, the TCD signal peaks in the CO-TPD experiment could not differentiate the desorbed gas(es), e.g., CO or CO_2.

Based on the results of the reaction tests displayed in Table 2, the selectivity of CO_2 increases over the catalysts with higher Cu promoter contents. This could be explained by the desorption peak in region I of the CO-TPD profiles (Fig. 2) of the catalyst that shows lower CO desorption

amounts for the catalysts with higher Cu contents. As the Cu content increases, the catalysts may adsorb less linear-type CO but more bridged-type CO, hence generating more CO_2 during the reaction tests from the disproportionation of the latter. Based on the stoichiometry of the disproportionation reaction reported [38, 39], the bridged-type CO disproportionation to CO_2 could also generate carbon deposits, but this was not analysed in this work.

The amount of CO adsorbed over the catalysts depends on active metal sites and adsorption stoichiometry. The adsorption of CO over Cu is weaker than that over Co [31]. Interestingly, in this work, the addition of a small fraction of Cu promoted the adsorption of CO, but higher Cu contents led to a significant decrease in CO adsorption (Fig. 2 and Table 1). This can be explained by the fact that with higher Cu contents, the Cu nanoparticles decorate the surface of the Co nanoparticles and cover them, which leads to lower amounts of CO adsorption over these catalysts [31]. In contrast, the CO adsorption amount was the highest in the catalyst with the low Cu loading of 1.5%. This indicates an effective bimetal role of the catalyst.

Furthermore, the shift of the desorption peaks to higher temperatures in the case of the Cu-promoted catalysts shows an enhanced strength of the bond between CO and the catalysts, which implies a higher CO bonding ability because of the presence of Cu. This strong CO bonding with the Cu-promoted Co/TNR catalysts can be explained by the synergistic CO adsorption, which is found to be the main factor leading to the increased activity of the 1.5Cu-Co/TNR catalyst. This is consistent with the reported work for Cu-promoted Co/Al_2O_3 catalyst [40]. In synergistic CO adsorption, the carbon atoms of CO adsorb on Co, while the oxygen atoms adsorb on Cu [41, 42].

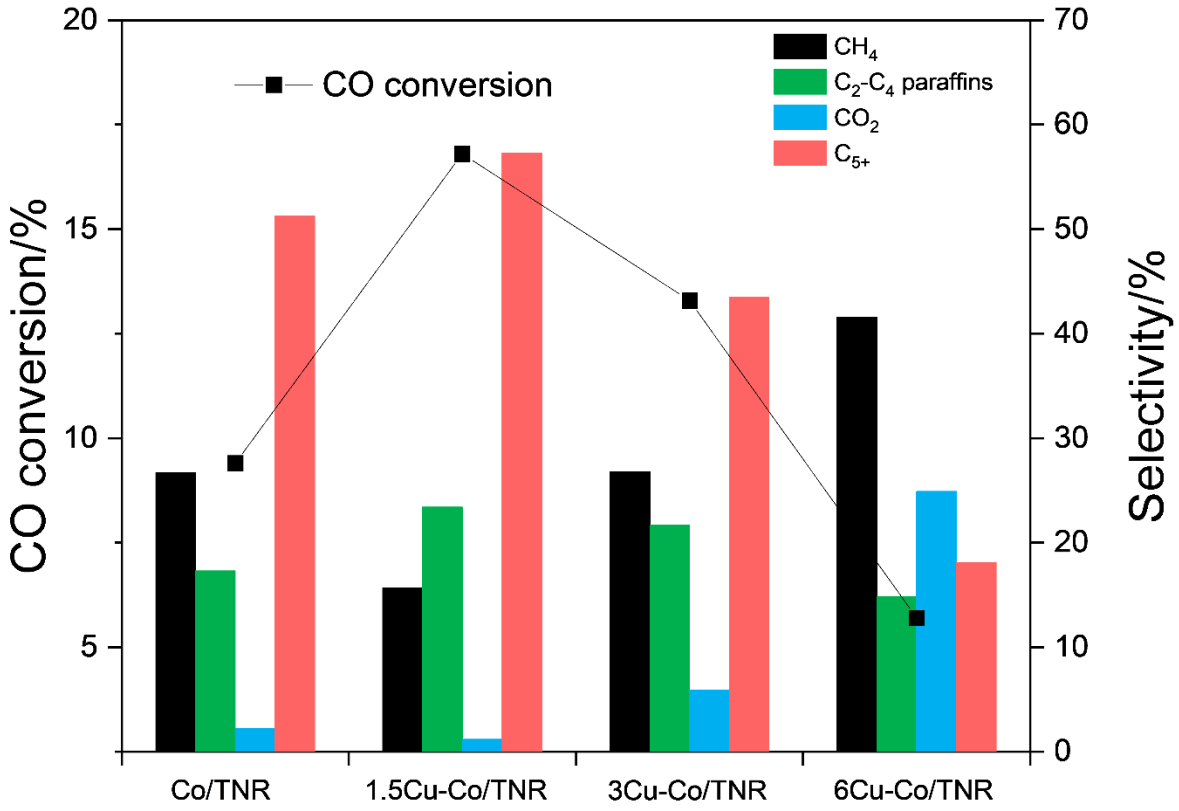

Fig. 5 CO conversion and product selectivity for Co/TNR and Cu-promoted Co/TNR catalysts. FTS conditions: H_2/CO = 2, 6000 mL/(g_{cat}.h), T= 240 °C, P = 5 bar.

The synergistic CO adsorption and reducibility can also be used to explain the variations in product selectivity between the base Co/TNR and the 1.5Cu-Co/TNR catalyst. For example, the selectivity of methane and CO_2 is suppressed over the 1.5Cu-Co/TNR catalyst due to improved reducibility and enhanced synergistic CO adsorption. Typically, methane formation could occur via two pathways in CO hydrogenation: (1) direct dissociation of CO followed by successive C hydrogenation; (2) hydrogenation of CO followed by deoxygenation of CH_xO. Although pathway (1) is considered more favourable kinetically and the overall methane formation is endothermic, pathway (2) is suppressed in the 1.5Cu-Co/TNR catalyst as Cu doping may increase the energy barrier of methane formation from the co-adsorbed "CO + 4H". This is consistent with the report given for the Cu-doped Fe(100) surface, where Cu

doping lowers the adsorption energies of all species (formed during CO hydrogenation) on the potential energy surfaces [43].

In addition, it can be inferred that the 1.5% Cu does not cover the Co active sites to a significant extent. For the promoted catalysts containing more than 1.5% Cu (i.e., 3Cu-Co/TNR and 6Cu-Co/TNR), the effect of the Cu covering the Co active sites could be observed, resulting in lower CO conversion due to the decrease in Co active sites. However, the covering of the Co active sites by the Cu promoter has resulted in enhanced selectivity of methane and CO_2 compared with the 1.5Cu-Co/TNR catalyst. This finding is in agreement with the work reported for Al_2O_3-supported Co-based catalysts [23]. Furthermore, the higher contents of Cu also promoted the WGS reaction, which contributed to the higher selectivity of methane and CO_2 [41]. It can be concluded that in catalysts with higher Cu contents, Cu covers the surface of the Co active metal, and the catalysts lose the synergistic effect of CO adsorption. This results in the loss of both the catalytic activity and the selectivity of C_{5+} hydrocarbons.

The best two catalysts were further tested at a higher temperature (300 ℃) to investigate the effect of temperature on the catalytic activity results. The results in Table 2 clearly show an increase in the CO conversions over both the 1.5Cu-Co/TNR and 3Cu-Co/TNR catalysts, but the product selectivity was also affected by the higher reaction temperature. The CO conversion increased from 16.8 and 13.3% to 25 and 19.6% over the 1.5Cu-Co/TNR and 3Cu-Co/TNR catalysts, respectively. A higher selectivity of methane and CO_2 but a lower selectivity of paraffins and C_{5+} hydrocarbons were observed, which suggests that the Cu-Co/TNR catalysts promote the WGS reaction at higher temperatures [1, 44, 45].

Co and Cu nanoparticle-based supported and unsupported catalysts with promoters such as K, Rb, Cs, Ca, Na and Ru have been widely reported for CO hydrogenation reactions [46-49]. Comparison of the results published in the literature reveals that CO conversion (16.8%) and

C_{5+} selectivity (57.5%) achieved over the 1.5Cu-Co/TNR catalyst surpassed the Cu-Co-based catalysts supported on TiO_2 (promoted with 2.5% each of K, Rb and Cs) [46], as shown in Table 3. Notably, these promoted catalysts [46] were tested at 250 ℃ with a H_2/CO ratio of 3 and two times the amount of Cu and Co as in the 1.5Cu-Co/TNR catalyst. The best catalyst in this work (1.5Cu-Co/TNR) outperforms the Co-based catalysts promoted with expensive noble metals, such as ruthenium (Ru) [49], by producing a higher C_{5+} yield at the same reaction temperature while operating under half the reaction pressure used previously [49]. Moreover, the 1.5Cu-Co/TNR catalyst also shows a higher C_{5+} yield than the unsupported Mn-promoted Co-based catalyst [48]. A comprehensive investigation at the molecular level, for example, by means of DFT calculations, is required to provide more insight into the mechanism behind the outstanding performance of the 1.5Cu-Co/TNR catalyst.

Table 3 Comparison of the current work with previously reported literature.

Catalyst	**Temp. (℃)**	**Pressure (bar)**	**H_2/CO**	**CO conv. (%)**	**C_{5+} Selectivity (%)**	**Ref.**
1.5Cu-Co/TNR	240	5	2	16.8	57.5	This work
2.5%K-30%(CoCu)/TiO_2				10.8	20.3	
2.5%Rb-30%(CoCu)/TiO_2	250	50	3	8.4	16.8	[46]
2.5%Cs-30%(CoCu)/TiO_2				13.4	9.5	
5%Ca-15%Co/SiC	240	20	2	13	5	[47]
Co_3Mn_1–Na_2O	240	10	2	20	42	[48]
i-5Co0.05RuAl	240	10	2	9.6	69.7	[49]

4 Conclusions

The effect of the Cu promoter in Co/TNR catalyst was investigated for the FTS reaction. The reduction profiles of the Cu-promoted catalysts showed that Cu doping enhanced the reducibility of the catalysts and, subsequently, the catalytic activity. The CO and H_2 adsorption capacities were observed to be the highest for the 1.5Cu-Co/TNR catalyst among the catalysts tested in this work, which also showed the highest CO conversion and C_{5+} hydrocarbon selectivity at 240 ℃ and 5 bar. The increase in the reaction temperature to 300 ℃ showed an increase in CO conversion from 16.8% and 13.3% to 25% and 19.6% over the 1.5Cu-Co/TNR and 3Cu-Co/TNR catalysts, respectively. The methane and CO_2 selectivity was found to increase with reaction temperature, which is in accordance with the previously reported literature. The enhanced activity of the 1.5Cu-Co/TNR catalyst was associated with the synergistic mechanism of the CO interaction with the catalyst surface, where the carbon atoms adsorb on the Co sites and the oxygen atoms adsorb on the Cu sites. The operation stability and and reusability of the catalysts need to be further investigated before industrial applications. Theoretical studies, such as DFT calculations, would be useful to further identify the possible reaction pathways.

Acknowledgements

The authors would like to thank the financial support from the Ministry of Business, Innovation & Employment in New Zealand under the MBIE Endeavour “Smart Ideas” grant (UOCX1905) and the China Scholarship Council (CSC). This work was also supported by the publication scholarship offered by the College of Engineering at the University of Canterbury. This is a post-peer-review, pre-copyedit version of an article published in Catalysis Letters. The final authenticated version is available online at: http://dx.doi.org/10.1007/s10562-020-03506-3.

References

[1] Khodakov AY, Chu W, Fongarland P (2007) Chem Rev 107: 1692–1744.

[2] Jahangiri H, Bennet J, Mahjoubi P,Wilson K, Gu S (2014) Catal Sci Technol 4: 2210–2229.

[3] Gholami Z, Tisler Z, Rubas V (2020) Catal Rev https://doi.org/10.1080/01614940.2020.1762367

[4] Yang J, Ma W, Chen D, Holmen A, Davis BH (2014) Appl Catal A:Gen 470: 250–260.

[5] Savost'yanov AP, Eliseev OL, Yakovenko RE, Narochniy GB, Maslakov KI, Zubkov I, Soromotin VN, Kozakov AT, Nicolskii AV, Mitchenko SA (2020) Catal Lett 150: 1932–1941.

[6] Gholami Z, Zabidi NAM, Gholami F, Ayodele OB, Vakili M (2017) Rev Chem Eng 33: 337–358.

[7] van Steen E, Claeys M (2008) Chem Eng Technol 31: 655–666.

[8] Madon RJ and Seaw H (1977) Catal Rev 15: 69–106.

[9] Iglesia E, (1997) Appl Catal A-Gen 161: 59–78.

[10] Di Z, Feng X, Yang Z, Luo M (2020) Catal Lett https://doi.org/10.1007/s10562-020-03158-3

[11] Chou W, Wu P, Luo M, Li W, Li S (2020) Catal Lett 150: 1993–2002.

[12] Yang Z, Luo M, Liu Q, Shi B (2020) Catal Lett https://doi.org/10.1007/s10562-020-03147-6

[13] Marion MC, Hugues F (2007) Stud Surf Sci Catal 167: 91–96.

[14] Luque R, de la Osa AR, Campelo JM, Romero AA, Valverde JL, Sanchez P (2012) Energy Environ Sci 5: 5186–5202.

[15] Haryanto A, Fernando SD, Pordesimo LO, Adhikari S (2009) Biomass Bioenergy 33: 882–889.

[16] Lualdi M, Logdberg S, Regali F, Boutonnet M, Jaras S (2011) Top Catal 54: 977–985.

[17] Davis BH (2007) Ind Eng Chem Res 46: 8938–8945.

[18] Rofer-DePoorter CK (1981) Chem Rev 5: 447–474.

[19] Tsakoumis NE, Ronning M, Borg O, Rytter E, Holmen A (2010) Catal Today 154: 162–182.

[20] Bartholomew CH (2001) Appl. Catal. A: Gen. 212: 17–60.

[21] Morales F, Weckhuysen BM (2006) Catalysis 19: 1.

[22] Ma WP, Kugler EL, Dadyburjor DB (2011) Energy Fuel 25: 1931–1938.

[23] Jacobs G, Ribeiro MC, Ma WP, Ji YY, Khalid S, Sumodjo PTA, Davis BH (2009) Appl Catal A-Gen 361: 137–151.

[24] X.B. Chen, S. Cao, X.L. Weng, H.Q. Wang, Z.B. Wu, Effects of morphology and structure of titanate supports on the performance of ceria in selective catalytic reduction of NO, Catal. Commun., 26 (2012) 178-182.

[25] F.J. Song, Y.X. Zhao, Q. Zhong, Adsorption of carbon dioxide on amine-modified TiO_2 nanotubes, J. Environ. Sci., 25 (2013) 554-560.

[26] M. Kim, S.H. Hwang, S.K. Lim, S. Kim, Effects of ion exchange and calcinations on the structure and photocatalytic activity of hydrothermally prepared titanate nanotubes, Cryst. Res. Technol., 47 (2012) 1190-1194.

[27] Khan WU, Chen SS, Tsang, DCW, Teoh WY, Hu X, Frank LYL, Yip ACK (2020) Nano Res 13: 533–542.

[28] Yu XF, Wu NZ, Xie YC, Tang YQ (2000) J Mater Chem 10: 1629–1634.

[29] Guo XZ, Huang J, Wang SR, Wang YM, Zhang BL, Wu SH (2009) J Disper Sci Technol 30: 1114–1119.

[30] Tang XL, Zhang BC, Li Y, Xu YD, Xin Q, Shen WJ (2004) Catal Today 93-5: 191–198.

[31] Mo XH, Tsai YT, Gao J, Mao DS, Goodwin JG (2012) J Catal 285: 208–215.

[32] Baharudin L, Severinsen I, Yip ACK, Golovko VB, Watson MJ (2020) Chem Eng J 389:124399

[33] Ernst B, Bensaddik A, Hilaire L, Chaumette P, Kiennemann A (1998) Catal Today 39: 329–341.

[34] Arnoldy P, Moulijn JA (1985) J Catal 93: 38–54.

[35] Sexton BA, Hughes AE, Turney TW (1986) J Catal 97: 390–406.

[36] Chen W, Zijlstra B, Filot IAW, Pestman R, Hensen EJM (2018) ChemCatChem 10: 136–140.

[37] Tsyganenko AA, Mardilovich PP (1996) J Chem Soc Faraday Trans 92: 4843–4852.

[38] Gopalakrishnan R, Viswanathan B (1984) J Colloid Interface Sci 102: 370–372.

[39] Gopalakrishnan R, Viswanathan B (1984) Surf Technol 23: 173–177.

[40] Sitthisa S, Resasco DE (2011) Catal Lett 141: 784–791.

[41] Reddy BM, Reddy GK, Rao KN, Khan A, Ganesh I (2007) J Mol Catal A-Chem 265: 276–282.

[42] Maity S, James OO, Chowdhury B, Auroux A (2014) Curr Sci India 106: 1538–1547.

[43] Tian X, Wang, T, Yang Y, Li YW, Wang J, Jiao H (2017) Appl Catal A-Gen 530: 83–92.

[44] Keyser MJ, Everson RC, Espinoza RL (1998) Appl Catal A-Gen 171: 99–107.

[45] Dry ME (2002) Catal Today 71: 227–241.

[46] Shi Z, Yang H, Gao P, Chen X, Liu H, Zhong L, Wang H, Wei W, Sun Y (2018) Chinese J Catal 39: 1294–1302.

[47] Li Z, Wu J, Wu L (2017) React Kinet Mech Catal 122: 887–900.

[48] Xie J, Paalanen PP, van Deelen TW, Weckhuysen BM, Louwerse MJ, de Jong KP (2019) Nat Commun 10: 167.

[49] Park JY, Lee YJ, Karandikar PR, Jun KW, Bae JW, Ha KS (2011) J Mol Catal A: Chem 344: 153–160.